2015-09-08

Characterization of Residual Stress as a Function of Friction Stir Welding Parameters in Oxide Dispersion Strengthened (ODS) Steel MA956

Brewer, Luke N.; Bennett, Martin S.; Baker, B. W.; Payzant, E. Andrew]; Kolbus, Lindsay M.

Elsevier

Journal Name: Materials Science and Engineering. A, Structural Materials: Properties, Microstructure and Processing; Journal Volume: 647
http://hdl.handle.net/10945/60996

Characterization of Residual Stress as a Function of Friction Stir Welding Parameters in Oxide Dispersion Strengthened (ODS) Steel MA956

L.N. Brewer[*+], M.S. Bennett, and B.W. Baker
Naval Postgraduate School

E.A. Payzant and L.M. Sochalski-Kolbus
Oak Ridge National Laboratory

This article characterizes the residual stresses generated by friction stir welding of oxide dispersion strengthened steel MA956 over a series of welding conditions. A plate of MA956 steel was friction stir welded at three conditions: 500 rpm/25 millimeters per minute (mmpm), 400 rpm/50 mmpm and 400 rpm/100 mmpm. The residual stresses across these welds were measured using both x-ray and neutron diffraction techniques. Longitudinal residual stresses up to eighty percent of the yield strength were observed for the 400 rpm/100 mmpm condition. Increasing the traverse rate while holding the rotational speed fixed increased the residual stress levels in the stir zone and at the stir zone-thermomechanically affected zone interface. The stress profiles displayed the characteristic "M" shape, and the asymmetry between advancing and retreating stress peaks was limited, occurring mainly on the root side of the weld. The large magnitude of the stresses was maintained throughout the thickness of the plates.

Key words: ODS steel, residual stress, friction stir welding, x-ray diffraction, neutron diffraction

[*] To whom all correspondence should be addressed: lnbrewer1@eng.ua.edu
[+] L.N. Brewer is now an associate professor in the Metallurgical and Materials Engineering Department at the University of Alabama.

I. Introduction.

Despite the promise of oxide dispersion strengthened (ODS) steels for use in high temperature nuclear applications, joining these materials through traditional, fusion-based welding is highly problematic. The microstructural attributes that give this steel its strength can be severely degraded by fusion welding techniques. Processes like gas tungsten arc welding and gas metal arc welding result in transport and agglomeration of the finely dispersed oxides to the surface of the weld pool, as well as significant alterations to the grain sizes upon solidification[1]. The result is a significant reduction in yield strength across the weld and degraded creep properties in the large HAZ outside the weld pool. Other processes like electron beam welding and laser beam welding give similar results, coarsening and agglomerating of the oxide particles that give ODS steels their strength [2, 3].

Friction stir welding (FSW) shows significant promise as a solid-state joining technique for ODS steels. FSW involves the insertion of a hard, rotating tool into the surface of the pieces to be joined. The tool rotation heats the material to approximately eighty-ninety percent of the melting point of the alloy. The tool is then translated across the specimen, thus joining the material. This process does not melt the base metal, and preserves many of the mechanical and microstructural properties that make ODS steels attractive. Several authors have successfully demonstrated friction stir welding on ODS steels[4-9]. While defect-free welds can be achieved in ODS steels by FSW, some evolution in the stir zone microstructure has been observed; including an increase in ferrite grain size, an increase in oxide particle size, and a resultant reduction in hardness/yield strength for the stir zone material[4, 5, 9, 10].

Although FSW can significantly reduce the distortion that often accompanies fusion welding, the process can generate significant residual stresses. For most alloys, longitudinal (parallel to the weld) residual stress profiles across the weld line display an ‘M’ shape, with tensile maxima occurring in the thermomechanically affected zone (TMAZ) just beyond the tool shoulder. Moving from the TMAZ into the base metal, the tensile stresses rapidly decrease and are balanced by compressive stresses. In the stir zone itself, the longitudinal stresses are reduced from the peak values at the TMAZ but are generally still tensile. This reduction in stress level may be caused by evolution of the microstructure, which results in a much lower yield strength in the stir zone of the weld [10, 11]. In FSW of AA5083, Peel [12] showed that longitudinal

residual stresses can reach up to 40% of the yield strength in the stir zone, where FSW reduced the 0.2% offset yield strength in the stir zone (SZ) from 392 MPa in the base metal to 147 MPa at the weld center line. FSW modeling by Chen [13]and Bastier [14]predicted that the maximum longitudinal stresses are 40-50% of yield strength in AA7050 and 6061-T6 respectively. Experimental work performed by Steuwer et al. [15]on HSLA-65 steel demonstrated a peak longitudinal residual stress over 80% of the nominal yield strength. Reynolds [11]observed a similar phenomenon in SS304 where the maximum longitudinal residual stress was 80% of yield for some conditions. In the ODS steel PM2000, Mathon [7] performed a neutron diffraction-based, residual stress analysis for a single (600 RPM, 50 mmpm) FSW condition and found that the longitudinal residual stresses on the advancing side of the weld can be as high as 50% of the yield strength of the base metal. Stresses of this magnitude are significant as they can drastically reduce the fatigue life of friction stir welded components.

This paper examines the residual stress distributions generated from FSW of MA956 plate over several welding conditions. We will compare the surface residual stress values with the internal plate values by comparing x-ray and neutron diffraction data. Of importance is the interplay between the evolution of the microstructure during FSW and the distribution of residual stresses afterwards.

II. Experimental Methods.

The material used in these experiments consisted of two plates of MA956, a high Cr, ferritic, oxide dispersion strengthened (ODS) alloy/steel produced by Special Metals Inc. Its chemical composition is listed in Table 1.

C	Cr	Al	Ti	Y_2O_3	Mo	Mn	Ni	S	Si	P	Fe
0.023	19.93	4.75	0.39	0.51	0.02	0.09	0.04	0.008	0.08	0.006	Bal.

Table 1. **Measured chemical composition of MA956 (all elements in weight percent_. From [4]**

The processing and FSW of these plates were accomplished as detailed in the work by Baker et al. [4]. The alloy was canned and extruded at 1100°C and hot rolled three times at

1100°C over a period of 4 hours with reheating to 1100°C for 30 minutes before and after each rolling. The final plate was machined to a thickness of 4 mm.

Friction stir welding was performed by MegaStir Technologies using a 25 mm diameter MS 80 grade polycrystalline cubic boron nitride (PCBN) tool with a convex scroll shoulder step spiral (CS4). The plunge force was a constant 17.8 kN. Three different conditions were selected to test the residual stress distribution across a range of heat inputs. From highest to lowest heat input: 500 rpm/25 millimeters per minute (mmpm), 400 rpm/50 mmpm, 400 rpm/100 mmpm. These FSW conditions correspond to rotational to traverse rate ratios of 20, 8, and 4, respectively. As all of the other FSW parameters (FSW machine, tool geometry, plunge force, etc.) were held constant except for the welding rotation and traverse rates, it is assumed in this paper that the heat inputs during welding increased, in order, from 400/100 to 400/50 to 500/25. In each case, it is assumed that there is a relative increase in heat input although we did not measure the absolute value during the experiments. These welds were all performed in one pass, changing conditions mid-pass.

X-RAY DIFFRACTION

The x-ray residual stress measurements were performed with the iXRD Residual Stress Analyzer from Proto Manufacturing. The residual stress measurements were made using the traditional d-spacing versus $\sin^2\psi$ technique[16]. All residual stress measurements were performed with Cr x-rays (λ=2.291 Å), produced at an x-ray tube power of 20 kV and 4.0 mA, under the conditions listed in Table 2:

{hkl} reflection	ferrite {112}
Bragg angle for diffraction (2θ)	156.31°
Number of exposures per ψ angle	5
Time per exposure	5 seconds
Beam aperture diameter	1 mm
ψ Angles	±36.8°, ±31.9°, ±27.3°, ±20.6°, ±13.2°, ±13.2°, ±11.8°, ±10.5°, ±8.2°, ±3.7°, ±3.1°

ψ oscillation	±4°

Table 2. **X-ray residual stress measurement conditions.**

Alignment of the x-ray diffractometer was confirmed using a stress-free ferrite powder and a peened steel calibration sample (from Proto Manufacturing, -502 ± 35 MPa) prior to measuring residual stresses on the plate. Residual stress measurements were collected at 5mm increments across the weld from the base metal (BM) to the thermo-mechanically affected zone (TMAZ) (Figure 1). To provide better spatial resolution, 1 mm increments were used across the TMAZ and the stir zone (SZ). Figure 1 shows the positions of residual stress measurements, taken approximately at the midpoint of each welding condition to ensure steady state welding conditions were established. Line A corresponds to the 500 rpm/25 mmpm condition, line B corresponds to the 400 rpm/50 mmpm condition, and line C corresponds to the 400 rpm/100 mmpm condition.

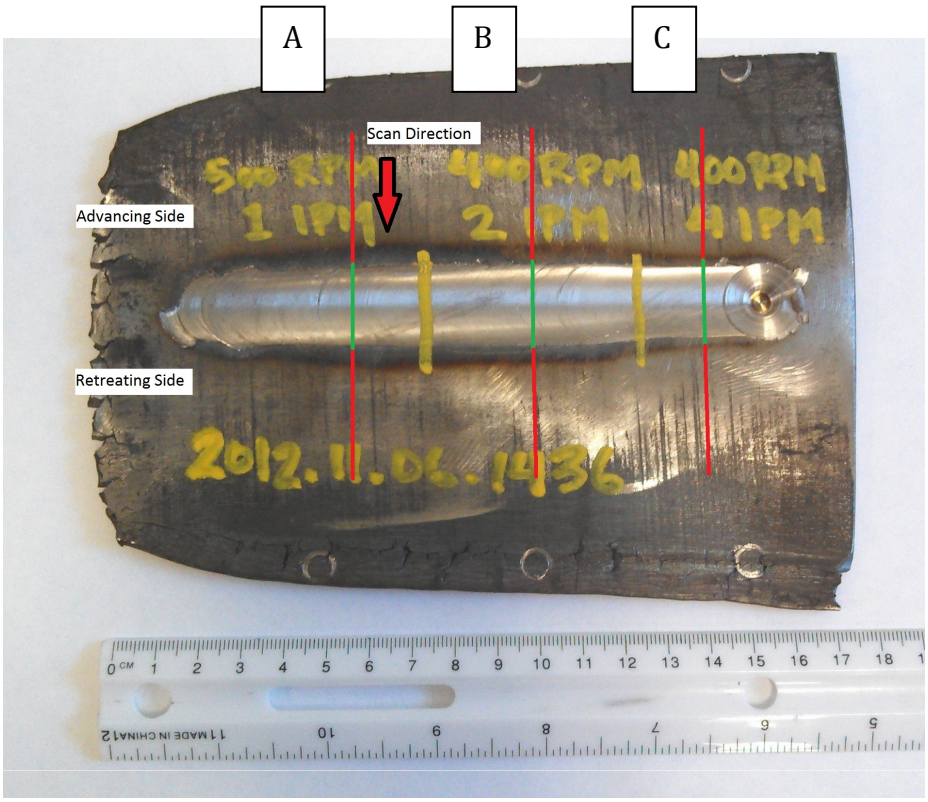

Figure 1. Geometry of x-ray residual stress measurements on friction stir welded plate. Note that the red line portions had spacing between analysis points of 5 mm, while the

green line portion had a spacing of 2 mm.

Residual stress measurements were also collected as a function of depth. Electropolishing was utilized to remove material at four depths up to ~1 mm in two locations: 2 mm outside of the stir zone and along the weld centerline. Both of these measurements were made on the 400 rpm/ 100 mmpm section of the friction stir weld. Electropolishing was performed with Proto Manufacturing's 'Electrolyte A' at an applied voltage of 50 V with a resultant current of 2.2-3.0 A for approximately 160 s to reach each depth. The depth was measured using the auto-focusing pointer on the iXRD, accurate to approximately 0.01 mm.

NEUTRON DIFFRACTION:

Neutron diffraction strain mapping [17] experiments were performed at the Neutron Residual Stress Facility (beam line HB-2B) at the High Flux Isotope Reactor (HFIR) [18]. A double-focusing silicon monochromator was oriented to achieve a neutron wavelength of ~1.733Å, which locates the ODS ferritic steel {112} reflection at ~ 94° 2θ (*i.e.*, near 90° to obtain a nearly cubic gauge volume). The incident beam was defined by a 1 mm wide x 5 mm high cadmium slit, and the diffracted beam slit was also 1mm wide, located 20 mm from the sample, as illustrated in Figure 2. The 5 mm long dimension was oriented along the weld direction to increase the sample volume so that data could be collected quickly. For the longitudinal strain mapping direction, the incident beam height was restricted to 1mm, the smaller volume requiring proportionally longer counting times.

The sample was mounted to the sample stage with 80/20 aluminum in 2 different orientations (Figure 3). The sample was aligned in each orientation optically to a precision of ±0.2 mm, following which selected locations were verified to ±0.1mm using neutron "edge scans" to ensure that the gauge volume was fully buried in the sample at all measurement locations. This step was particularly necessary as the FSW sample was not flat, due both to rolling stresses in making the plates, and residual stresses from the FSW process. The weld line was not perfectly straight, and the width of the HAZ depended on the FSW parameters, so an estimate

was made of the length of the region of interest and the collected data were later manually corrected so that the center of each weld line was defined to be at x=0.

Data were collected for three orthogonal orientations (i.e., normal, longitudinal, and transverse with respect to the weld line), at selected points along lines at the center of each set of weld parameters (400/100, 400/50, and 500/25). Initial measurements of the 500/25 section of the weld indicated that the residual stresses had clearly been altered by the layer removal in the nearest electropolished region, as discussed in the previous section, and so a second line was measured further from the electropolished region to avoid this. The strain-free lattice parameter "d-zero" value was established by measuring the peak position at a location at a corner of the sample far from the weld line where the residual stress was deemed likely to be small. This is the "far-field reference" discussed in Hutchings [17]. In addition, re-measurement of the peak position at this location every time the sample was remounted confirmed that the instrument parameters remained constant. The d-zero value was subsequently refined in the data analysis to achieve reasonable force balance, as discussed in Hutchings [17].

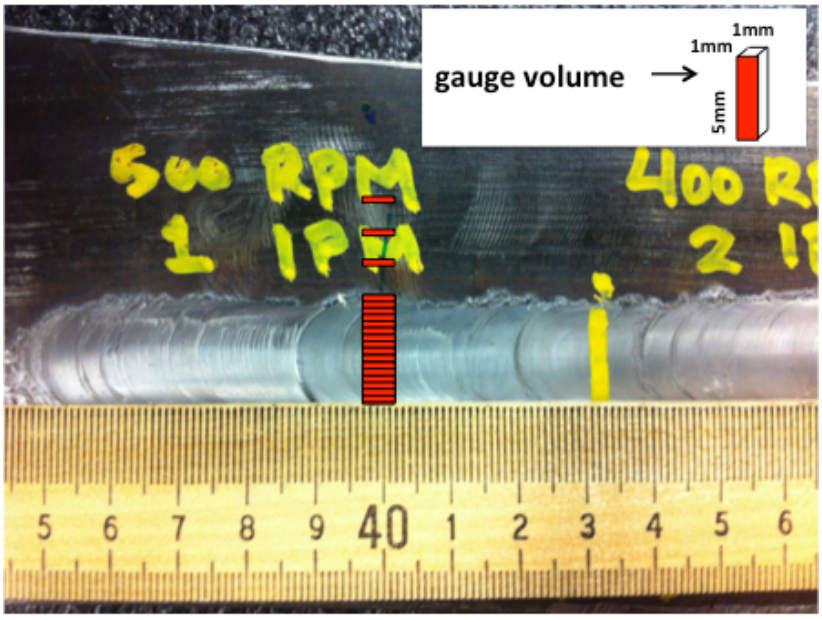

Figure 2. Geometry and placement of gauge volume for neutron diffraction measurements. Gauge volume was 1x5x1 mm for transverse and normal directions, but was 1x1x1 mm for longitudinal direction. Data was collected every 1 mm in weld region and every 4-5 mm outside of the weld.

Figure 3. Figure 3. Geometry for neutron diffraction at HFIR HB2B beam line. (Left) geometry for transverse strain meausrement. The strains normal to the plate were measured by rotating the sample 90° about the weld axis. (Right) geometry for longitudinal strain measurement

RESULTS

X-RAY DIFFRACTION RESIDUAL STRESS PROFILES:

Each of the measured x-ray residual stress profiles on the crown side of the plate showed the "M" profile with varying degrees of intensity (Figure 4). Peak longitudinal stresses occurred just beyond the weld nugget and tool shoulder, and were balanced by compressive stresses in the heat affected zones (HAZ) and base metal (BM). The profile was least pronounced for the highest heat input condition, 500/25, but as the heat input decreased, the "M" shape became more apparent. Residual stress peaks on the advancing and retreating sides were nearly equal in magnitude.

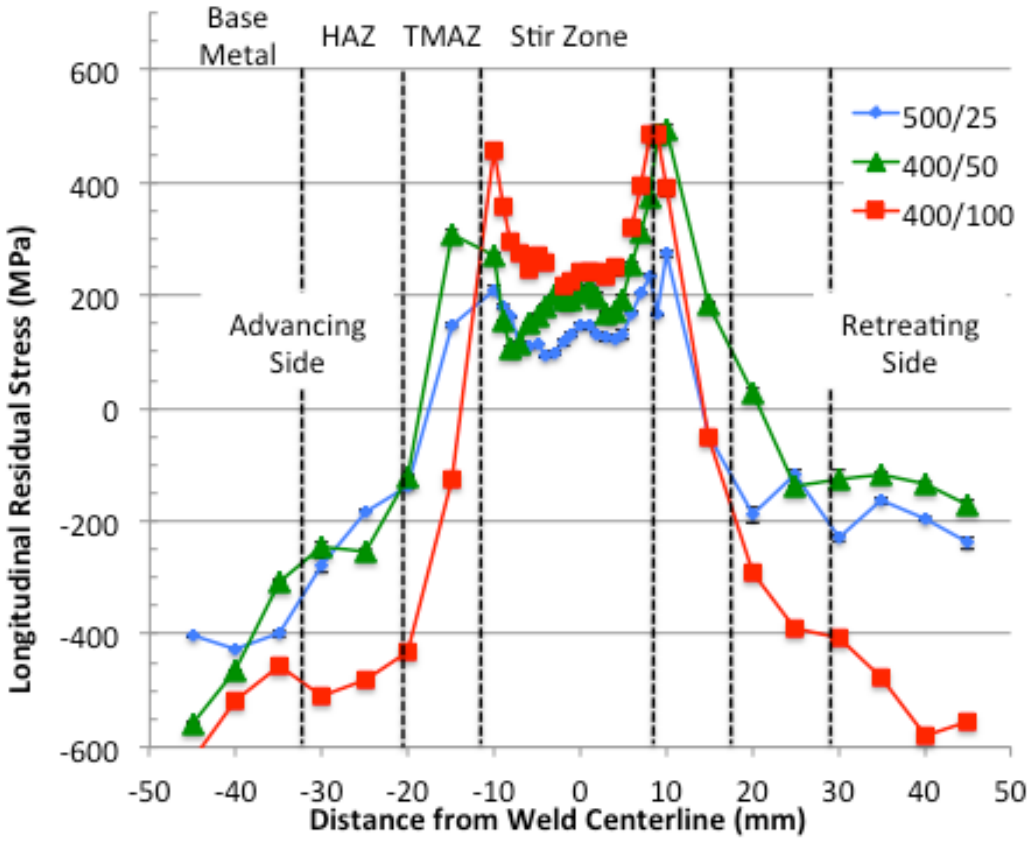

Figure 4. Longitudinal residual stresses measured by x-ray diffraction from the crown side of the plate. Note that the positions of the TMAZ and HAZ are approximate.

A more detailed view of the spatial gradient in longitudinal stress confirmed that the largest stresses were generated by the lowest heat input (Figure 5). Even with better spatial resolution on the advancing side, asymmetry between the peak stresses was not observed on the crown side of the plate.

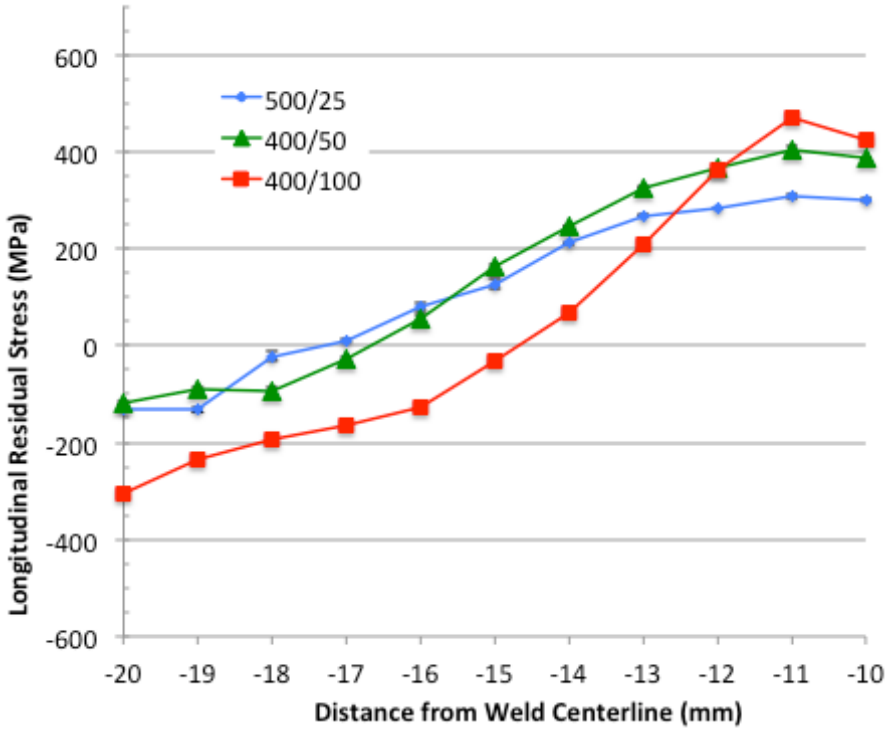

Figure 5. Longitudinal residual stresses (x-ray diffraction) near the TMAZ on the crown side of the plate, on the advancing side of the friction stir weld (negative values for position always indicate advancing side of the weld nugget).

Transverse stresses on the crown side of the plate also increased with lower heat input. In the stir zone region, residual stress values ranged from -10 MPa (nearly zero) for the 500/25 condition to +233 MPa for the 400/100 condition (Figure 6). As expected, the transverse stresses were lower than the longitudinal stresses at the same point on each plate, but followed the same trends as longitudinal stresses. Interestingly, the transverse stresses evolved in more of a "W" pattern than the "M" pattern observed for the longitudinal stresses. More asymmetry in stress between the advancing and retreating sides of the weld was observed for the transverse stress distributions.

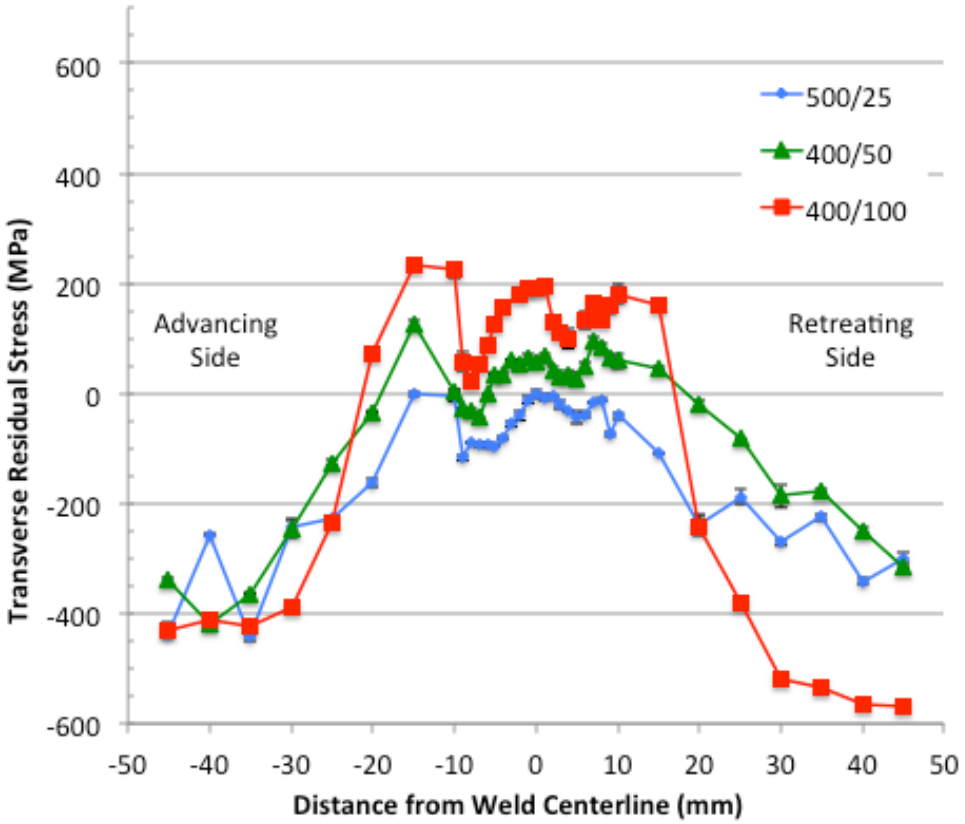

Figure 6. Transverse stresses (x-ray diffraction) from the crown side of the plate.

The residual stresses measured as a function of depth from the crown surface showed a consistent level of residual stress for the first several hundred microns below the surface (Figure 7). At the weld centerline (stir zone), the longitudinal stresses did not change significantly down to a depth of 1 mm below the surface. In contrast, the longitudinal stresses near the TMAZ decreased significantly with depth. From 900 MPa at the surface, the longitudinal stress peak decreased to less than 600 MPa. This abrupt change is likely due to the abrupt change in microstructure. As see in Figure 7, the shape of the weld nugget is at an angle to the plate surface. As one takes measurements with depth, the measurement volume will likely pass through a gradient in microstructure and therefore residual stress.

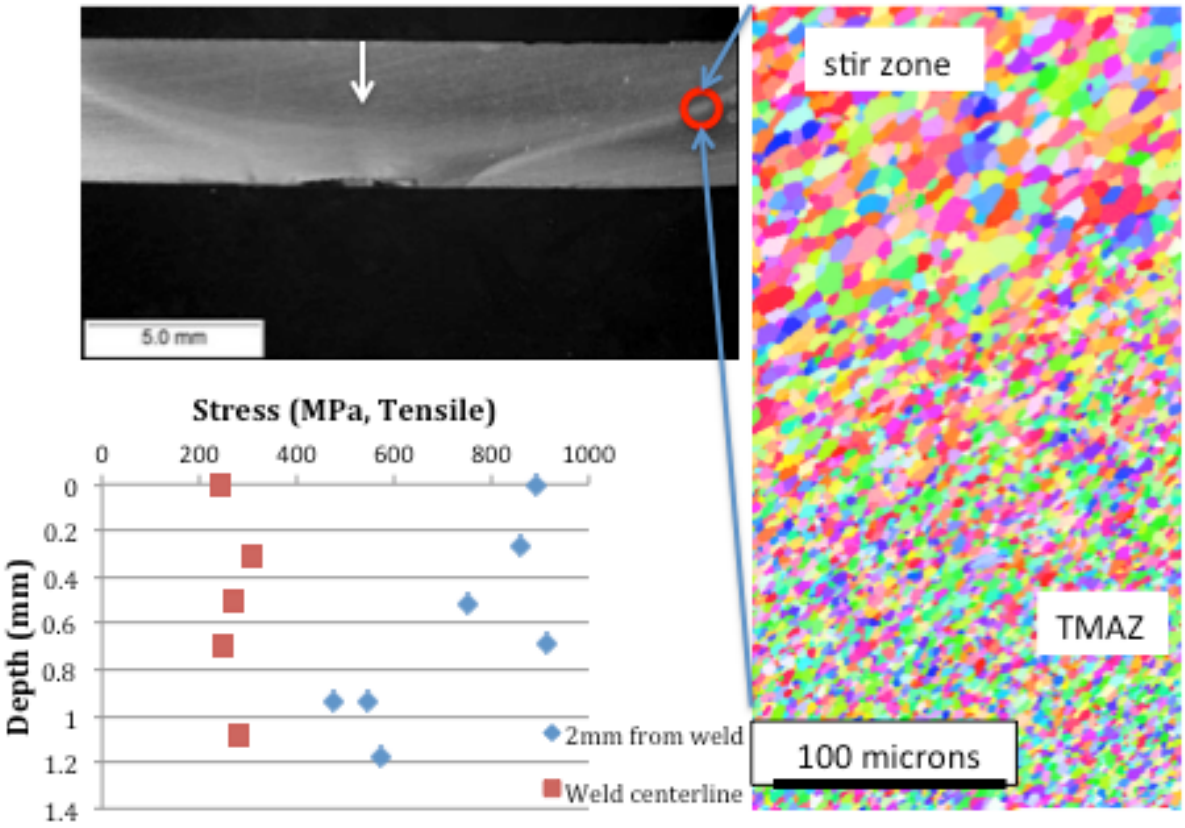

Figure 7. Longitudinal stresses (x-ray diffraction) with as a function of depth for the 400/100 condition. The optical macrograph shows a cross section of the friction stir weld. The white arrow indicates the approximate location of the depth profile in the center of the stir zone (red squares). The data from the TMAZ (blue diamonds) was taken just off the right hand side of this macrograph. The image to the right is an inverse pole figure map of the boundary between the stir zone and the TMAZ for this weld, showing the abrupt change in grain size at this boundary. This orientation map is taken from Baker et al. 2014[19]

Measurements taken across the root side of the weld revealed distinct differences from those taken across the crown of the plate (Figure 8). The root-side profiles displayed the characteristic "M" shape, and again decreasing heat input generally resulted in larger residual stresses. However, more asymmetry was observed between stress peaks on the advancing and retreating sides. The 500/25 and 400/100 conditions had peak longitudinal stresses on the advancing side of 621 MPa and 402 MPa; respectively, while the peak stresses on the retreating side were nearly 140 MPa less for each case. Less asymmetry was observed for the 400/50 condition, where peaks on the advancing and retreating sides were only different by 70 MPa. Moreover, the magnitudes of the peak longitudinal residual stresses on the root side were more

than 100 MPa larger than those on the crown side of the plate. Lastly, the difference in stress level between the peak at the TMAZ and the center of the stir zone was qualitatively larger on the root side of the plate than on the crown side. It should be noted that the surface condition left by FSW at the center of the stir zone did not allow for reliable measurement of the residual stresses for a width of approximately 6 mm. These points have been intentionally omitted from Figure 8.

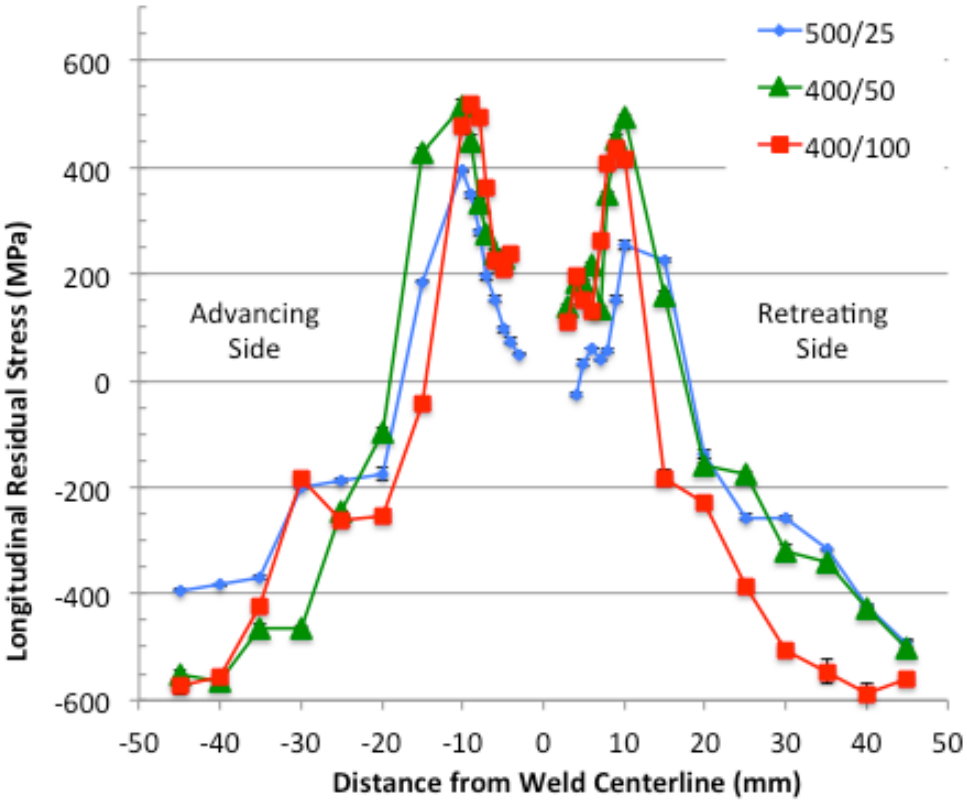

Figure 8. Longitudinal residual stress profiles (x-ray diffraction) from the root side of the plate. Note that several points right around the centerline have been removed due to unacceptable levels of surface roughness in these areas.

NEUTRON DIFFRACTION RESIDUAL STRESS PROFILES:

The neutron diffraction experiments produced similar residual stress profiles to those recorded by x-ray diffraction (Figure 9). The "M" shape profile was clearly observed for the longitudinal stresses, but not for the transverse or normal stresses. The level of longitudinal residual stress for the 400/100 condition was notably larger in the stir zone than for the other two

FSW conditions which were almost indistinguishable from the neutron diffraction measurements. The magnitude of the stresses agreed more closely with the larger stresses measured on the root side of the plate by x-ray diffraction. The normal stresses outside of the stir zone were very close to zero, indicating a plane stress configuration for the plate; however, the normal stresses inside of the stir zone were measurably tensile and uniform. Neutron diffraction-based residual stress profiles did not display much anisotropy between the peaks on the advancing versus retreating sides. The transverse residual stresses measured by neutron diffraction were primarily tensile and were relatively uniform across the weld region.

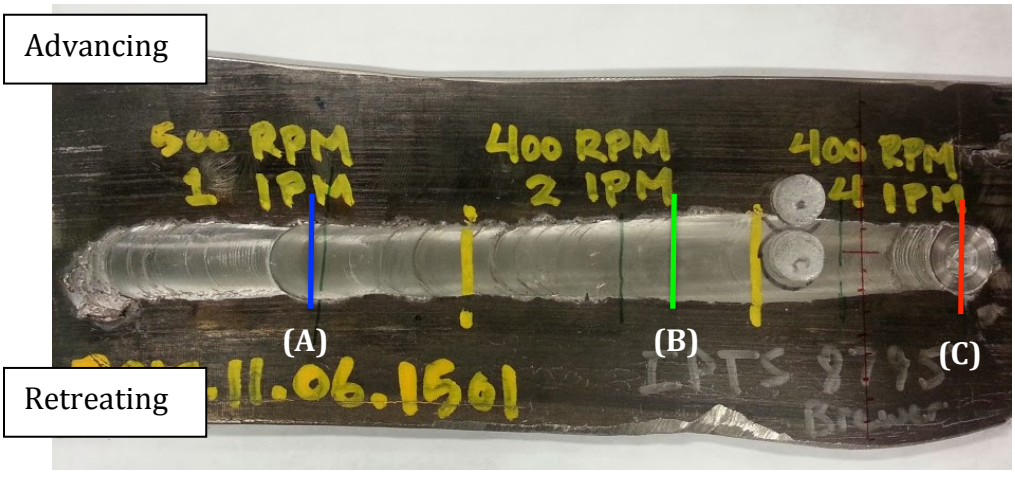

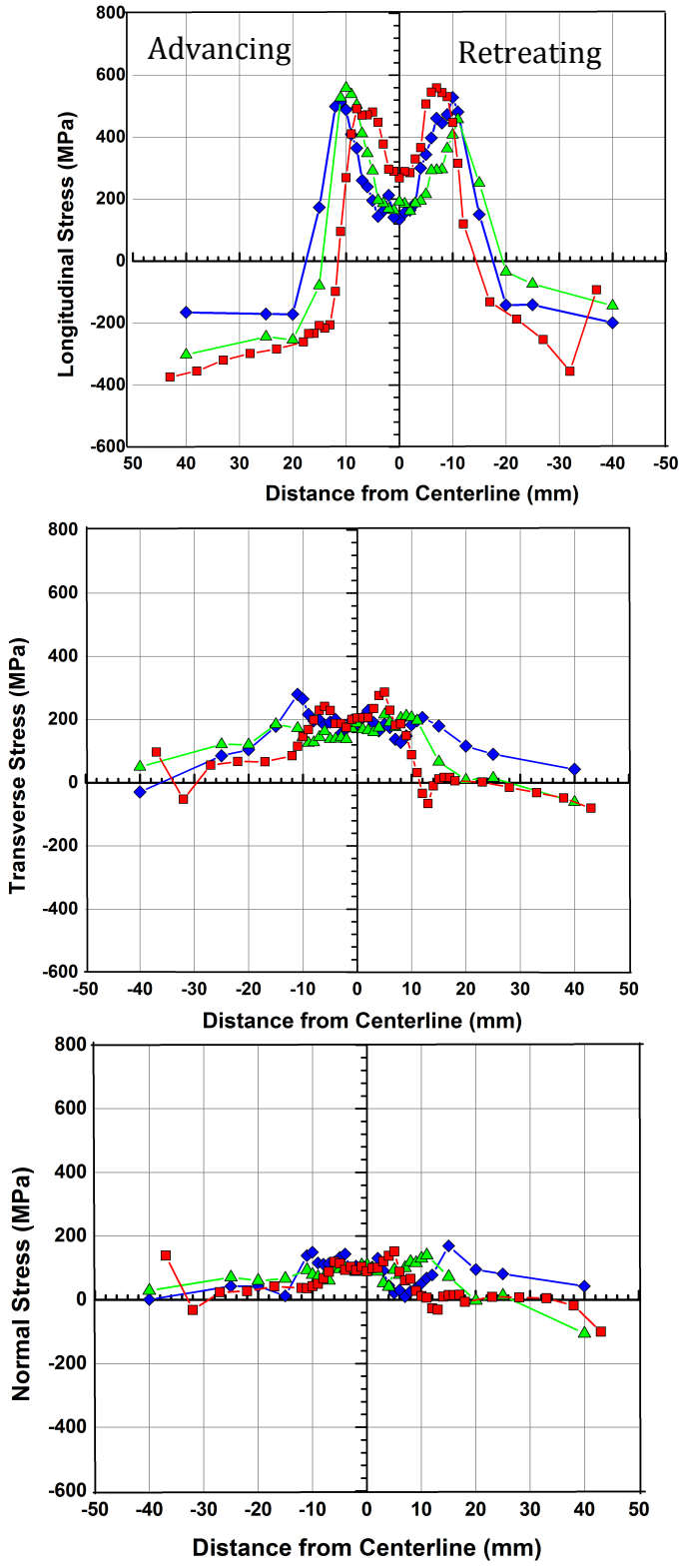

Figure 9. Residual stress profiles measured by neutron diffraction for each FSW condition. (A)Blue line and symbols represents 500/25 (B) Green line and symbols

represent 400/50 (C) red line and symbols represent 400/100.

The peak breadth from neutron diffraction (full width at half maximum) clearly showed the effects of friction stir welding (Figure 10). For each FSW condition, the peak breadth narrowed considerably in the stir zone compared with the base metal or the TMAZ. The peak breadth in the stir zone for all three FSW conditions possessed approximately the same value. Interestingly, the value on the advancing side of the stir zone was slightly higher than on the retreating side of the stir zone for all cases. In addition, the peak breadth in the advancing side TMAZ was larger for the 400/100 condition than the base metal or the other FSW conditions. The widths of the narrow peak regions did not vary meaningfully with heat input.

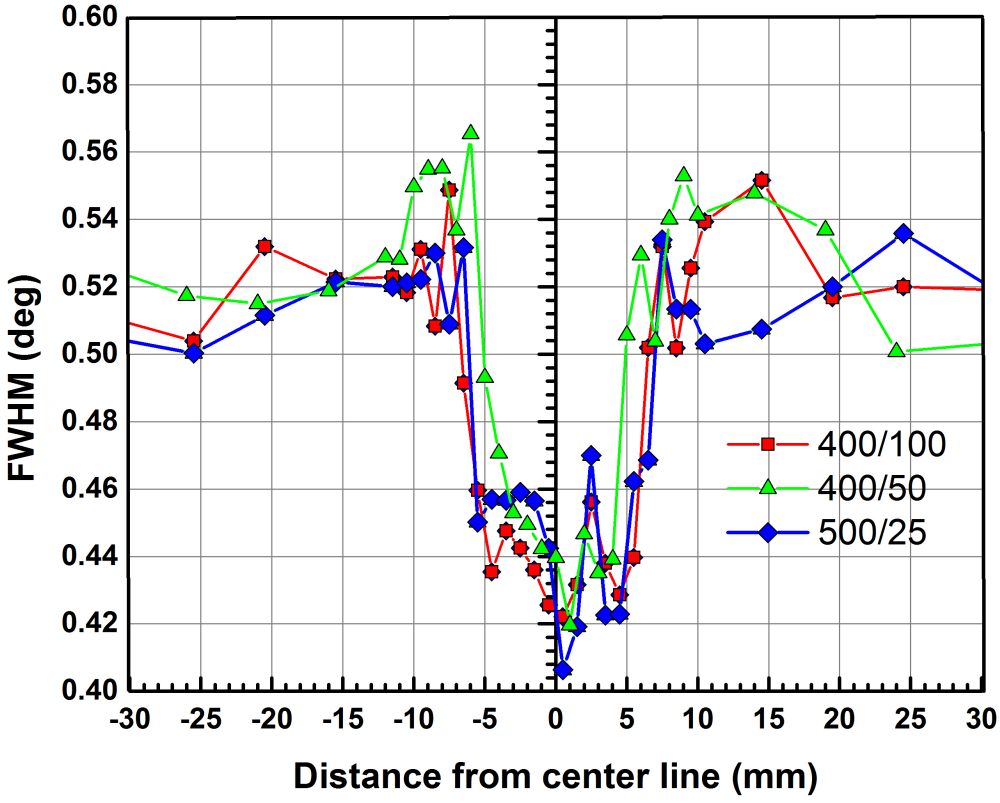

Figure 10. Spatial distribution of neutron diffraction peak full-width-at-half-maximum (FWHM) across the three welds for the stress measurements in the transverse direction. The trend seen here is similar for the longitudinal and normal directions. An empirical estimated error gave 0.05 degrees based on the mean of the FWHM of each measurement point subtracted from that of the Fe {211} standard powder measurement for HB-2B.

Discussion.

The magnitude of the longitudinal and transverse residual stresses measured in these experiments increased with decreasing heat input. While the heat input during FSW was not directly measured, it should scale with the ratio of the rotational speed to the transverse speed (given a fixed plate material, tool type and geometry, and plunge force). [20, 21] These rotational to traverse speed ratios are 20, 8, and 4 for the 500/25, 400/50, and 400/100 conditions respectively. So we see from Figures 3, 5, 7, and 8 that the magnitude of the residual stresses decreased as this ratio became larger. Furthermore, the residual stress level increased between the 400/50 and 400/100 conditions as the traverse speed increased. This connection between residual stress level and traverse speed has been clearly described by Steuwer using synchrotron x-ray diffraction measurements on friction stir welded HSLA-65 steel. [15] The surface residual stresses were notably different from the crown side versus the root side of the weld with root side stresses being larger. The neutron diffraction measurements which were taken from the center of the plate were closer in magnitude to the root side of the plate. The reason for this difference in unclear but may be due to the presence of an anvil on the root side which can act as a thermal sink thus reducing the amount of time at elevated temperature available for thermal relaxation as the weld material cools. It should be noted that this steel should not experience any phase transformation over the temperature range during FSW..

The distribution and magnitude of residual stresses after FSW are closely connected to the change in microstructure in the material. In this study, the welds are all undermatched with respect to the base plate material. Baker has measured the microstructural attributes and the yield strength of the stir zone material under the same FSW conditions used here (Table 3). [10] The room temperature yield strength of this alloy has decreased by approximately 40% after FSW. This reduction in yield strength is caused primarily by the coarsening of the oxide particles and the growth of ferrite grains in the stir zone material. In addition, this material is recrystallized with a low dislocation density. This decrease in dislocation density is the cause for the reduction in the diffraction peak breadth in the stir zone (see Figure 10). With this reduction in yield

strength, the stir zone material cannot support residual stresses as large as the plate material, which is much stronger. It is important to account for this reduction in yield strength when considering the magnitude of the residual stresses. The longitudinal stress in the stir zone for the 400/100 condition is approximately 240 MPa (crown side). This stress is only 26% of the plate material yield strength, but it is 44% of the stir zone material yield strength. By plotting the ratio of the measured longitudinal residual stress to the measured yield strength of the plate material and the stir zone, it can be seen that the 500/25 condition actually generates stresses that are larger fraction of its yield strength in the stir zone than the 400/100 condition (Figure 11).

Weld Condition	Heat Index	Ferrite Grain Size (μm)	Average Oxide Particle Size (nm)	σ_{YS} (MPa)	σ_{UTS} (MPa)	Hardness
BM	-	0.890	8.1	909	991	(H_V)
400-100	4	6.94	166	539	696	346
500-25	20	12.5	343	530	698	225

Table 3. Summary of microstructural attributes and mechanical properties for friction stir welded MA956. Table modified from Baker et al. 2014 [10]

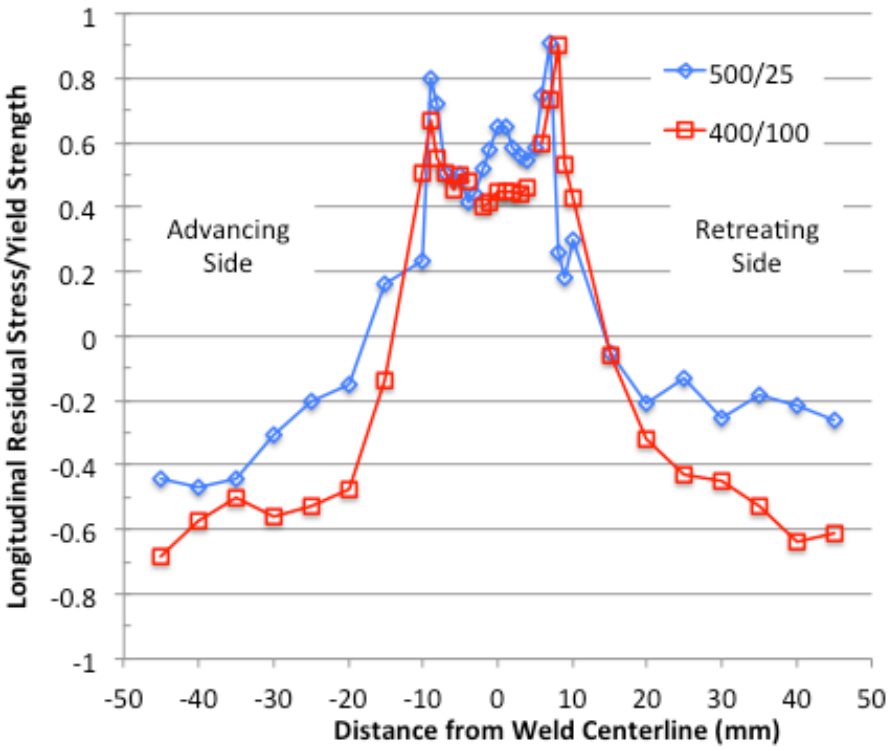

Figure 11. Distribution of longitudinal residual stresses normalized by yield strength for each weld microstructure. The stresses in the stir zone are normalized by yield strengths measured from actual friction stir welded material in work by Baker et al.

The nature of the particular steel and its microstructure can strongly affect the distribution and magnitude of residual stresses after FSW. The magnitude of longitudinal residual stress measured in this study is similar to that reported by Mathon on PM200, a very similar alloy to MA956. [7] Both studies show the "M" profile for longitudinal residual stresses; however, Mathon's results also show much larger transverse stresses that also possess the "M" profile. The neutron diffraction data in this paper show a relatively flat transverse stress profile, which is much lower in magnitude. Some care should be taken in a direct comparison because the FSW conditions in Mathon's work (600 RPM, 50 MMPM, 1.3 mm thick plate, possibly different tool geometries) are substantially different than the present conditions. In contrast, the work of Barnes and

Steuwer used very similar FSW conditions as those used in the current experiments, but on a different steel-HSLA65. [15, 20] The "M" profile is clearly visible for the longitudinal residual stresses. The magnitude of the longitudinal residual stresses are somewhat lower than those measured for MA956. It is important to note that the nominal yield strength of the HSLA65 is 450 MPa, compared with the 900 MPa yield strength of the MA956 material. While Barnes et al. do not report the yield strength of the stir zone material after FSW, they do show Vickers hardness values that are larger in the stir zone than those reported here. The difference is that HSLA65 forms martensite, bainite, and ferrite in the stir zone after FSW, thus making the material harder, and likely stronger, than the base plate material. As a third comparison, FSW of austenitic stainless steel (304LSS) produced a longitudinal residual stress distribution that did not show a clear "M" profile and was instead quite similar to the stress profile observed from fusion welding. [11]The point here is that FSW conditions alone cannot predict the residual stress distribution after welding; the type of steel and its phase transformations must be considered.

The effects of these residual stresses on the fatigue cracking behavior of the weld will likely be deleterious. A simple estimate of the impact of the residual stresses may be made by using the Goodman approach.[22] In this approach, a reduction in fatigue strength (amplitude stress (σ_a) for a fixed fatigue life), is related to the ratio of the mean stress (σ_m) to the ultimate tensile strength, σ_{UTS}. The original fatigue strength with no mean (or residual)stress is given by σ_o.

$$\sigma_a = \sigma_o \left(1 - \frac{\sigma_m}{\sigma_{UTS}}\right)$$

While no fatigue data exists for MA956, there is some limited information on PM2000, a very similar, commercial alloy. Chao et al. have measured the room temperature fatigue behavior of PM2000 after heat treatment.[23] Here, we will use the σ_o value given by Chao for as-received PM2000 plate, 320 MPa (N_f=10^8 cycles). The UTS values are from the measurements on stir zone material by Baker[10] and are given in Table 3. Using these values, we plot the predicted reduction in fatigue strength for MA956/PM2000 as a function of mean stress (Figure 12). The solid line shows the prediction using the larger

UTS value from the MA956 plate. The dashed line shows the prediction using the much reduced UTS value from the stir zone material under the 400/100 FSW condition. The window shown on Figure 12 gives the range of tensile residual (mean) stress values measured for the 400/100 FSW condition. As a reminder, the larger values occurred near the TMAZ while the SZ values were much lower. Even the lowest values measured decrease the fatigue strength to less than 250 MPa (a 22% reduction). The large difference between the solid and dashed curves shows the importance of accounting for the change in microstructure and mechanical properties between the plate material and the material in the welded region.

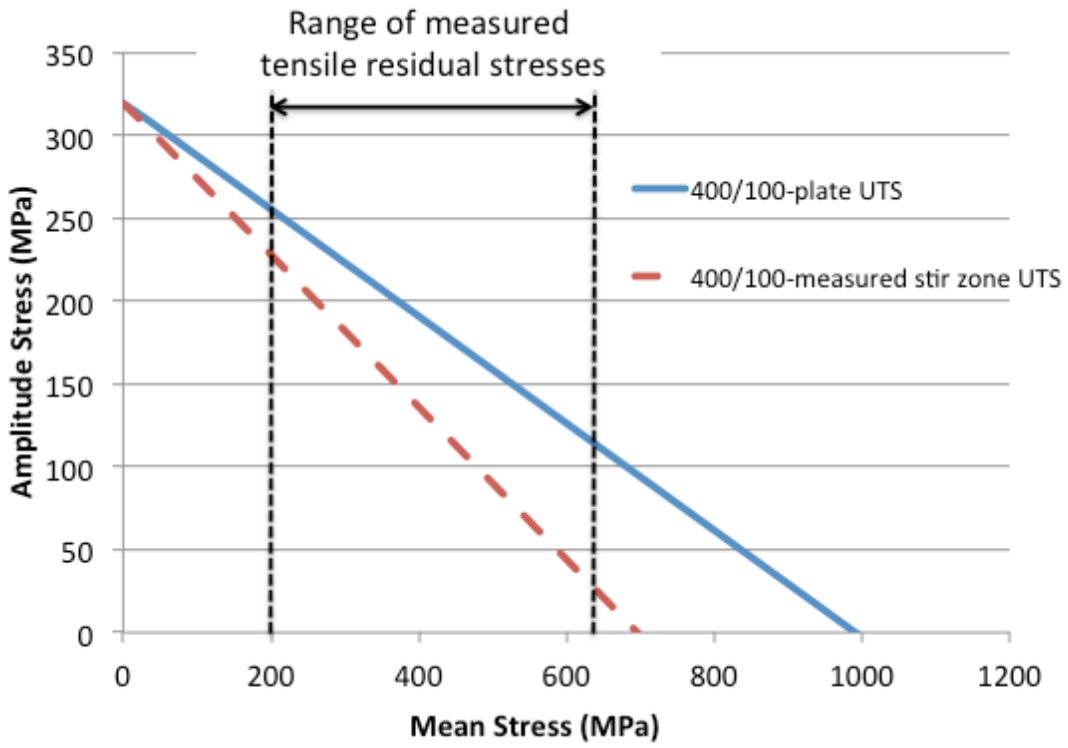

Figure 12. A Goodman plot ($N_f=10^8$ cycles at $\sigma_o=320$ MPa) for the friction stir weld of the 400/100 condition. The blue (solid) curve shows the reduction in fatigue strength with increasing mean stress using the UTS of MA956 plate. The red (dashed) curved shows the reduction in fatigue strength using the UTS measured from the stir zone of the weld under the 400/100 FSW condition.

Conclusions.

This article examines the use of x-ray and neutron diffraction to measure the distribution of residual stresses following FSW of MA956 ODS steel. Three FSW conditions were examined with an increasing ratio of the rotational to traverse speeds. Both x-ray and neutron diffraction recorded large, tensile residual stresses along the longitudinal direction of the friction stir welds. The longitudinal residual stresses were much larger than the transverse or normal residual stresses, and the residual stresses on the root surface of the weld were much larger than on the crown side. The magnitude of the residual stresses was inversely proportional to the ratio of the rotational to traverse speeds during welding. An increase in traverse rate increased the residual stress value measured. The x-ray and neutron diffraction data agreed well in the spatial distribution of stresses and the correlation of stress level with FSW parameters. The residual stresses measured were up to eighty percent of the plate value strength at the TMAZ and forty-fifty percent of the stir zone yield strength at the center of the stir zone.

Acknowledgements:

This work in part was performed under the auspices of the U.S. Department of Energy by Lawrence Livermore National Laboratory under Contract DE-AC52-07NA27344. The two plates measured in this study were provided by Lawrence Livermore National Laboratories. We are grateful for technical assistance from Dr. E.S.K. Menon at NPS.

Research conducted at ORNL's High Flux Isotope Reactor was sponsored by the Scientific User Facilities Division, Office of Basic Energy Sciences, US Department of Energy.

References:

[1] M.G. McKimpson, D. Odonnell, JOM-Journal of the Minerals Metals & Materials Society, 46 (1994) 49-51.
[2] R. Lindau, M. Klimenkov, U. Jaentsch, A. Moeslang, L. Commin, Journal of Nuclear Materials, 416 (2011) 22-29.
[3] H.J.K. Lemmen, K.J. Sudmeijer, I.M. Richardson, S. van der Zwaag, Journal of Materials Science, 42 (2007) 5286-5295.
[4] B.W. Baker, L.N. Brewer, E.S.K. Menon, T.R. McNelley, B. El-dasher, S. Torres, J.C. Farmer, M.W. Mahoney, S. Sanderson, Influence of Heat Input on Friction Stir Welding for the ODS Steel MA956, in: R.S. Mishra, M.W. Mahoney, S. Yutaka, Y. Hovanski, R. Verma (Eds.) Friction Stir Welding and Processing VII, Wiley, 2013.
[5] C.L. Chen, P. Wang, G.J. Tatlock, Materials at High Temperatures, 26 (2009) 299-303.
[6] D.T. Hoelzer, K.A. Unocic, M.A. Sokolov, Z. Feng, Journal of Nuclear Materials, 442 (2013) S529-S534.
[7] M.H. Mathon, V. Klosek, Y. de Carlan, L. Forest, Journal of Nuclear Materials, 386 (2009) 475-478.
[8] J. Wang, W. Yuan, R.S. Mishra, Journal of Nuclear Materials, 442 (2013) 1-6.
[9] J. Wang, W. Yuan, R.S. Mishra, I. Charit, Journal of Nuclear Materials, 432 (2013) 274-280.
[10] B.W. Baker, T.R. McNelley, L.N. Brewer, Materials Science and Engineering-A, 589 (2014) 217-227.
[11] A.P. Reynolds, W. Tang, T. Gnaupel-Herold, H. Prask, Scripta Materialia, 48 (2003) 1289-1294.
[12] M. Peel, A. Steuwer, M. Preuss, P.J. Withers, Acta Materialia, 51 (2003) 4791-4801.
[13] C.M. Chen, R. Kovacevic, Proceedings of the Institution of Mechanical Engineers Part B-Journal of Engineering Manufacture, 220 (2006) 1359-1371.
[14] A. Bastier, M.H. Maitournam, F. Roger, K. Dang Van, Journal of Materials Processing Technology, 200 (2008) 25-37.
[15] A. Steuwer, S.J. Barnes, J. Altenkirch, R. Johnson, P.J. Withers, Metallurgical and Materials Transactions a-Physical Metallurgy and Materials Science, 43A (2012) 2356-2365.
[16] I.C. Noyan, J.B. Cohen, Determination of Strain and Stress Fields by Diffraction Methods, in: Residual Stress: Measurement by Diffraction and Interpretation, Springer-Verlag, New York, 1987, pp. 117-162.
[17] M.T. Hutchings, P.J. Withers, T.M. Holden, T. Lorentzen, Practical Aspects of Strain Measurement Using Neutron Diffraction, in: Introduction to the Characterization of Residual Stress by Neutron Diffraction, CRC Press, Boca Raton, FL, 2005, pp. 149-202.
[18] H. Xu, C.R. Hubbard, K. An, Z. Feng, X.-L. Wang, J. Qu, Advanced Engineering Materials, 11 (2009) 650-653.
[19] B.W. Baker, E.S.K. Menon, T.R. McNelley, L.N. Brewer, B. El-dasher, J.C. Farmer, S. Torres, M.W. Mahoney, S. Sanderson, Metallurgical and Materials Transactions E, in press (2014).

[20] S.J. Barnes, A.R. Bhatti, A. Steuwer, R. Johnson, J. Altenkirch, P.J. Withers, Metallurgical and Materials Transactions A-Physical Metallurgy and Materials Science, 43A (2012) 2342-2355.
[21] L.Y. Wei, T.W. Nelson, Welding Journal, 90 (2011) 95S-101S.
[22] M.A. Meyers, K.K. Chawla, Fatigue, in: Mechanical Behavior of Materials, Cambridge University Press, New York, NY, 2009, pp. 719-721.
[23] J. Chao, J.L. Gonzalez-Carrasco, C. Capdevila, Iron and Steel Institute of Japan International, 47 (2007) 1214-1220.